Journal of The Electrochemical Society, **165** (2) B27-B33 (2018)
0013-4651/2018/165(2)/B27/7/$37.00 © The Electrochemical Society

One-Pot Biosynthesis of Reduced Graphene Oxide/Prussian Blue Microcubes Composite and Its Sensitive Detection of Prophylactic Drug Dimetridazole

Murugan Keerthi,[1] Muthumariappan Akilarasan,[1] Shen-Ming Chen,[1,*,z] Sakthivel Kogularasu,[1] Mani Govindasamy,[1] Veerappan Mani,[1,2,z] M. Ajmal Ali,[3] Fahad M. A. Al-Hemaid,[3] and M. S. Elshikh[3]

[1]*Department of Chemical Engineering and Biotechnology, National Taipei University of Technology, Taipei 106, Taiwan*
[2]*Institute of Biochemical and Biomedical Engineering, National Taipei University of Technology, Taipei 106, Taiwan*
[3]*Department of Botany and Microbiology, College of Science, King Saud University, Riyadh - 11451, Saudi Arabia*

Herein, a robust novel electrochemical sensor for the detection of prophylactic drug Dimetridazole (DMZ) has been developed eco-friendly through the green synthesis of reduced graphene oxide/Prussian blue microcubes (rGO/PB MCs), and the fabrication was economically done by efficient screen-printed carbon electrode (SPCE) modification method. It is critical as DMZ excess level in poultry farm imposes carcinogenic threats. A responsive, reproducible and long-lasting DMZ sensor was established using the material composed of Prussian blue microcubes encapsulated by thin sheets of reduced graphene oxide (rGO/PB MCs). The rGO/PB MCs composite is prepared through a facile hydrothermal approach, and its elemental, structural, electrochemical and catalyzing abilities are examined. The composite is fabricated on the SPCE, and the resulting improved electrode showed outstanding electrocatalytic ability toward DMZ and the reduction peak current are correlated to the DMZ concentrations. It retains the more extensive working range between 0.02 μM and 1360.1μM and the detection limit reaches 3.2 nM. It also possesses appreciable sensitivity of 2.2935 $\mu A \mu M^{-1} cm^{-2}$. This technique is efficiently applied to the detection of DMZ in spiked samples of milk and egg.
 [DOI: 10.1149/2.0591802jes]

Manuscript submitted October 23, 2017; revised manuscript received December 23, 2017. Published January 13, 2018.

1, 2-dimethyl-5-nitroimidazole (Dimetridazole) is a veterinary antibiotic drug belongs to 5-nitroimidazole type. It has been practiced to treat illnesses triggered by bacterial or protozoal infections in poultry.[1] When the carcinogenic, as well as the mutagenic properties of dimetridazole, was recognized, their consumption has been limited within the EU. As per the Committee Rule (EEC), 2377/90 of 1990, usage of DMZ as the prophylactic drug has been banned. Lately, due to another rule 2205/2001, DMZ is not legalized as a feedstuff preservative. Factually, DMZ drug has been withdrawn from the market. However, some countries including Australia, Canada, and Denmark permits the usage of DMZ.[2] Thus, the establishment of the reliable sensor device[3] is essential for the quick determination of DMZ. In contrast with other substantial analytical approaches, electroanalytical systems are reliable for DMZ detection due to its standard[4] and convenient instrumentations, and also it provides direct and rapid responses[5] as digital signals. Previously stated DMZ sensors are interfaced with gas chromatography[6] and liquid chromatography.[7] Nevertheless, developed modified electrodes has diminished the overpotential efficiently and noticeably reduced the fouling effect. Most of the earlier articles are concentrated on the recognition of DMZ in meat. In this, we equipped an active electrode, which is applicable for the detection of DMZ in milk and egg samples as well.

Graphene is one of the leading topics in electrochemistry for several decades due to its remarkable electronic and catalytic abilities.[8–11] Now, it has been believed that the electrocatalytic activities of graphene could be further elevated by modifying graphene with metal oxides as nanocomposites.[12–15] Mainly, graphene and cyano-metal nanocomposites are recently reported for its improved catalytic properties, and they are comprehensively applied in sensors and supercapacitors.[15–17] However, green synthesized rGO/PB microcubes (MCs) based composite has not once been applied in the field of electrochemical sensors.

Herein, we have described the green synthesis of PB microcubes embedded inside the thin sheets of rGO as a composite and applied for DMZ sensing (Figure 1). The sustainable preparation of the rGO/PB MCs composite from the mushroom extract is facile and does not necessitate any harmful solvents or reducing agents. The rGO/PB MCs film modified screen-printed carbon electrode (SPCE) revealed greater electrochemically active surface area, outstanding electrocatalytic ability and offered extraordinary sensitivity toward DMZ.

*Electrochemical Society Member.
[z]E-mail: smchen78@ms15.hinet.net; veera.678@gmail.com

Experimental

Materials and instrumentations.—Graphite (powder <20 μm), polyvinylpyrrolidone (PVP, K30), potassium hexacyanoferrate(II) are purchased and used as received. All the reagents taken were at its best grade for analysis and used without any further purification. The buffer solutions consumed for the electrochemical studies were 0.1 M phosphate buffer. The preparation methods of buffer solutions, chemical purchases, and instrumentation techniques are detailed in the supplementary data (SD-1).

Preparation of mushroom extract.—Fresh Volvariella volvacea (paddy straw mushroom) is purchased from PX-MART, Taiwan. Washed several times with deionized water to clean up the impurities on the surface and then chopped into smaller pieces. The chopped mushrooms are weighed (70 g) and taken in a sterilized borosilicate beaker (200 ml) filled with distilled water (150 ml) and boiled at 80°C for 3 h. Finally, the syrup-like filtrate is taken, cooled and used as an active reducing agent for further reactions.

Synthesis of rGO/PB MCs.—As shown in Scheme 1, Graphene oxide is synthesized from graphite by Hummers method. The rGO/PB MCs are prepared by a facile hydrothermal green approach. In Brief, 8.2 g of polyvinylpyrrolidone (PVP) was dissolved in 30 ml of 5mM potassium hexacyanoferrate (II) (pH 1), then 20 ml of mushroom extract (pH 1) was added slowly under magnetic stirring. Then, the solution is taken into a 100 mL Teflon bomb, which contains synthesized graphene oxide of 1 mg. Finally, the autoclave is sealed and maintained at 80°C for 12 h. The obtained product (rGO/PB MCs) is filtered and washed with distilled water and absolute ethanol, then dried under a vacuum drier at room temperature and the final product is taken for further characterizations.

Fabrication of rGO/PB MCs modified electrode.—The active surface area of the screen-printed carbon electrode is pre-cleaned by sweeping in the range between −1.0 V and 1.2 V (vs. Ag/AgCl), in pH 5 (0.1 M PB). Next, 8 μL rGO/PB MCs is drop cast on SPCE and

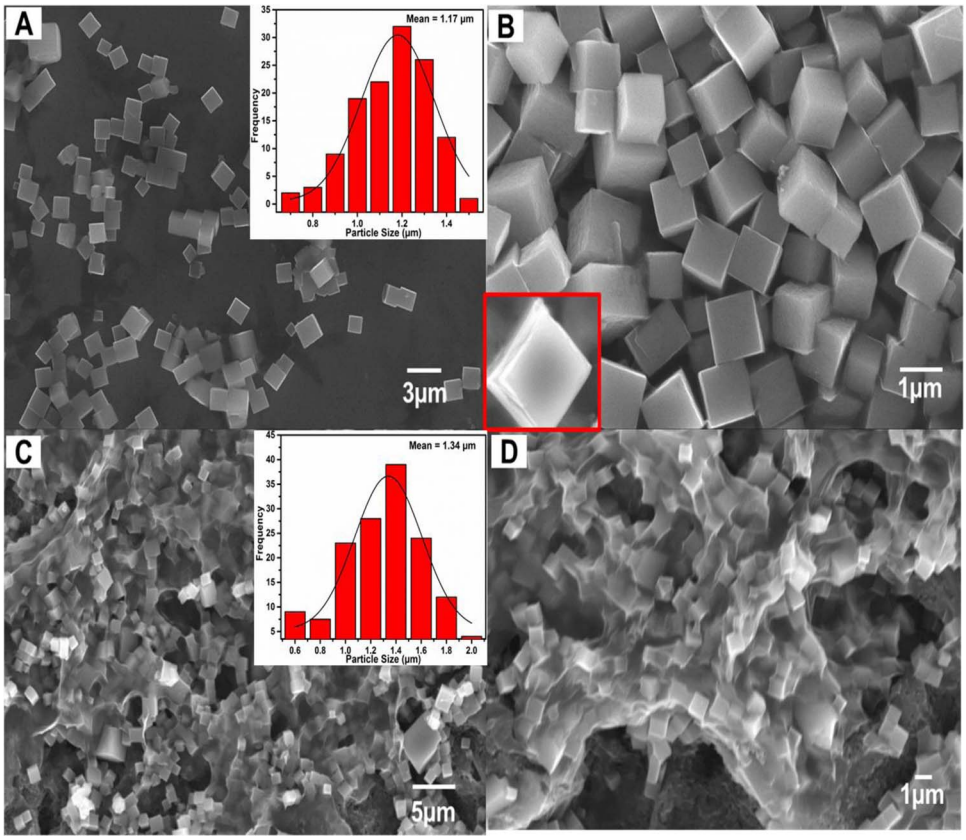

Figure 1. (A, B) FE-SEM images of PB MCs and (C, D) rGO/PB MCs. (Inset of A and C shows the particle size distribution profile of PB MCs and rGO/PB MCs and inset B shows the single cubic crystal).

dried at room temperature. As a control, rGO and PB MCs modified SPCEs are prepared.

Results and Discussion

Characterizations of rGO/PB MCs.—*Morphological and elemental characterizations.*—(Figure 1A and Figure 1B) Elucidated the FE-SEM images of Prussian blue (PB) cubes and that evidently exposed the statement of countless cube designed microparticles. The magnified image displayed the crystallinity of an individual cube, and the particle size ranged in micrometer (Figure 1B-inset). The microcubes are enclosed by the thin sheets of rGO, and every cube is connected under the sheets of rGO (Figure 1C, 1D). The existed elements(C, O, N, and Fe) in the composite are exhibited through EDX spectrum (Figure 2A) and weight proportions of (C, O, N, and Fe) are also indicated by the quantitative analysis (Figure 2B).

XRD and FT-IR.—(Figure 3A) Displayed the XRD pattern of graphene oxide and rGO/PB MCs. The GO pattern possessed an intense sharp peak at 11.02 Å (001). The composite rGO/PB MCs exhibited peaks at 17.6° (200), 24.9° (220), 31.8° (222), 35° (400), 38.8° (420), 42.1° (422), 50.2° (440), 54.7° (442), 57.8° (662), consistent with standard pattern of Prussian blue (JCPDS 01-073-0687). Obtained XRD spectrum is similar to the previously reported literature.[18]

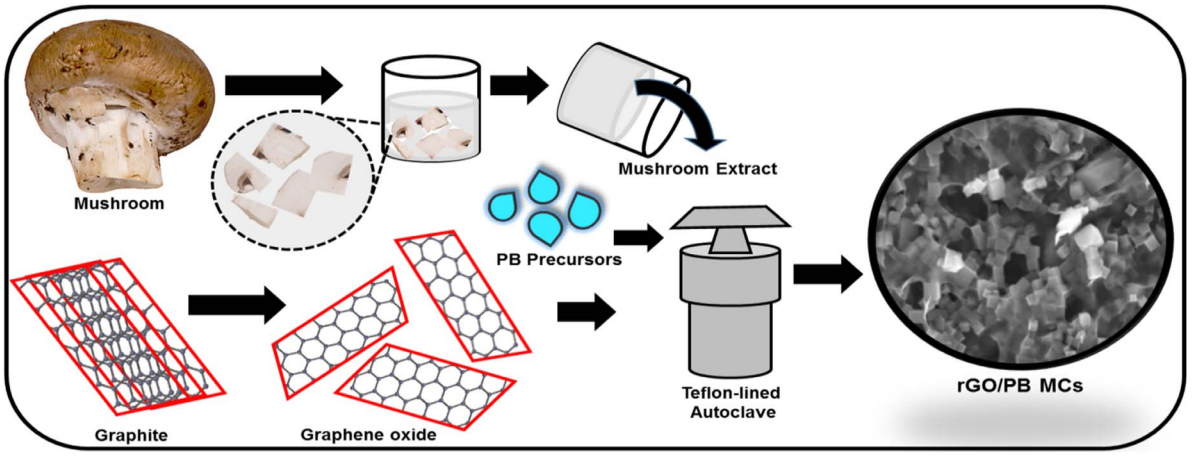

Scheme 1. Synthesis of rGO/PB MCs.

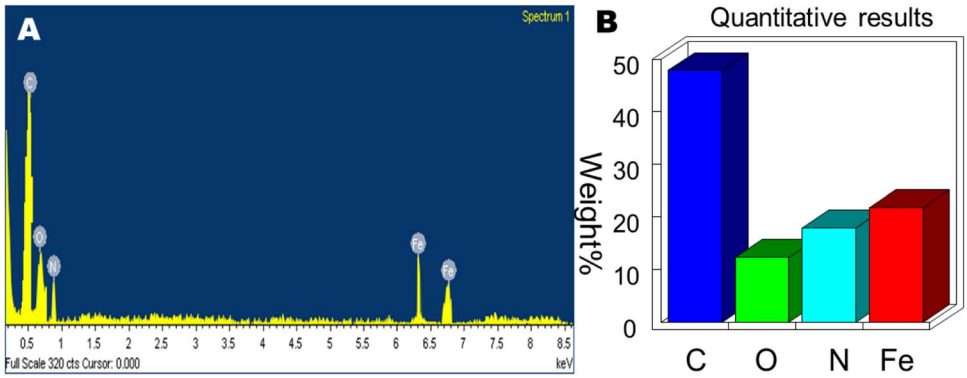

Figure 2. EDX spectrum (A) and Quantitative analyses of C, O, N, Fe (B).

Hence, the formation of crystalline PB MCs and rGO/PB MCs composite is confirmed.

With the purpose of defining the functional groups, FT-IR spectra of graphene oxide and rGO/PB MCs were studied (Figure 3B). The spectrum of rGO exhibited peaks at wavenumbers of 3417, 1763, 1682, 1391, 1087 and 1254 cm^{-1} which are associated to stretching vibrations of O−H, C=O, C=C, O−H, C−O, and C−O−C, respectively. However, the spectrum of rGO/PB MCs displayed a strong absorption band at 2079 cm^{-1}, which is correlated to the CN functional group ascending from the water responses near 3400 and 1590 cm^{-1} related with H-O-H bend and O-H stretch, respectively. In the far-infrared region, 509 cm^{-1} associated with Fe-C-N-Fe bending modes determines the characteristics of PB MCs. The obtained results are similar to the previous literature.[19] Therefore, the functional groups of PB MCs and rGO/PB MCs composite are confirmed.

Impedance study on rGO/PB MCs/SPCE.—(Figure 3C) displays EIS attained at bare SPCE (a), GO/SPCE (b) and rGO/PB MCs/SPCE (c) in 0.1 M KCl comprising 5 mM $Fe(CN)_6^{3-/4-}$. The experimental data are acquired by Randles equivalent circuit model (inset to Figure 3C), Where, R_{ct}, R_s, Z_w and C_{dl} were portraying charge transmission resistance, electrolyte resistance, Warburg impedance, and double layer capacitance, respectively. The subsequent order indicates the diameter of semicircles (i.e., R_{ct}); Bare SPCE (497.66 Ω)> GO/SPCE (399.02 Ω)> PB MCs/SPCE (239 Ω) > rGO/PB MCs/SPCE (70.14 Ω). Provided results indicate the lower resistance at rGO/PB MCs/SPCE, and it is kinetically facile over other electrodes.

Electrocatalysis of rGO/PB MCs/SPCE toward DMZ.—The CVs obtained at unmodified SPCE (a), GO/SPCE (b), PB MCs/SPEC (c), and rGO/PB MCs/SPEC (d) in pH 5 (PB) containing 50 μM DMZ at the scan rate of 50 mV s^{-1}, is demonstrated in (Figure 4A). The optical image of the system is visualized in *SD-2*. The following order reveals the electrocatalytic ability of these modified electrodes; rGO/PB MCs/SPCE > PB MCs/SPCE > GO/SPCE > Bare SPCE.

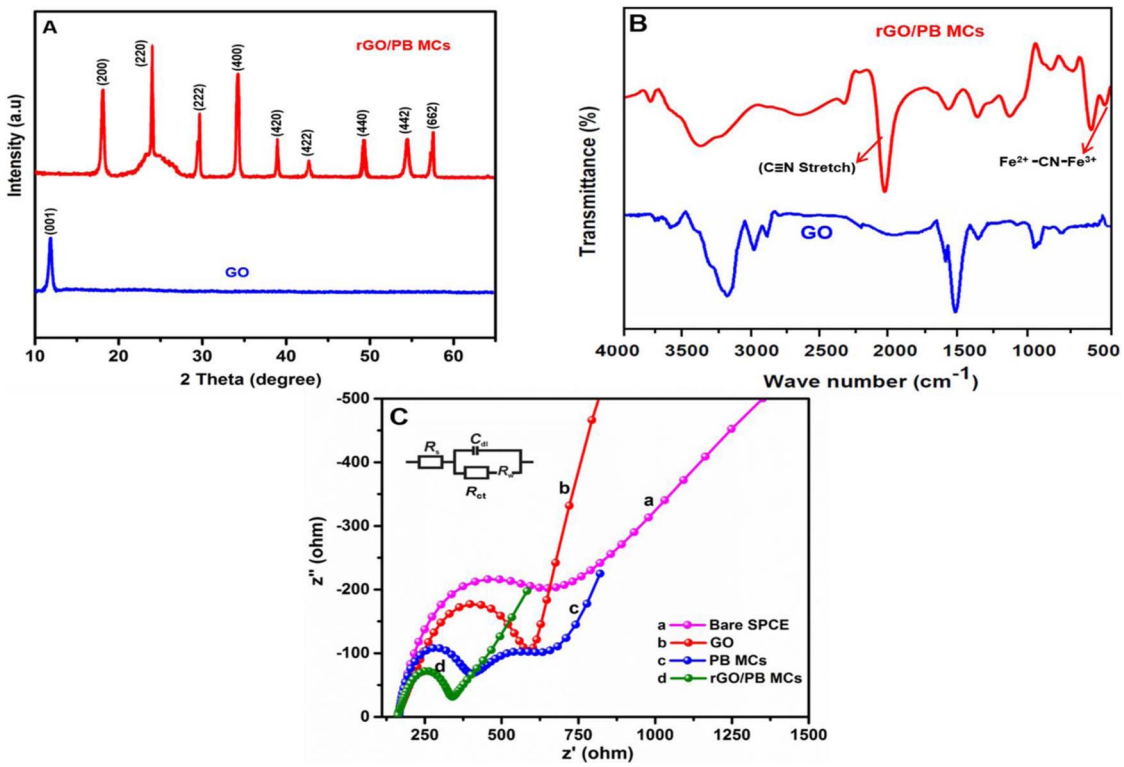

Figure 3. (A) XRD, (B) FT-IR spectra of GO and rGO/PB MCs and (C) EIS curves of bare SPCE (a), GO/SPCE (b), PB MCs/SPCE (c) and rGO/PB MCs/SPCE (d) obtained in 0.1 M KCl containing 5 mM $Fe(CN)_6^{3-/4-}$. Amplitude: 5 mV, Frequency: 0.1 Hz to 100 kHz. Inset: Randles equivalent circuit used to fit the data; *R*s, *R*ct, *C*dl, and *Z*w are electrolyte resistance, charge transfer resistance, double layer capacitance and Warburg impedance, respectively.

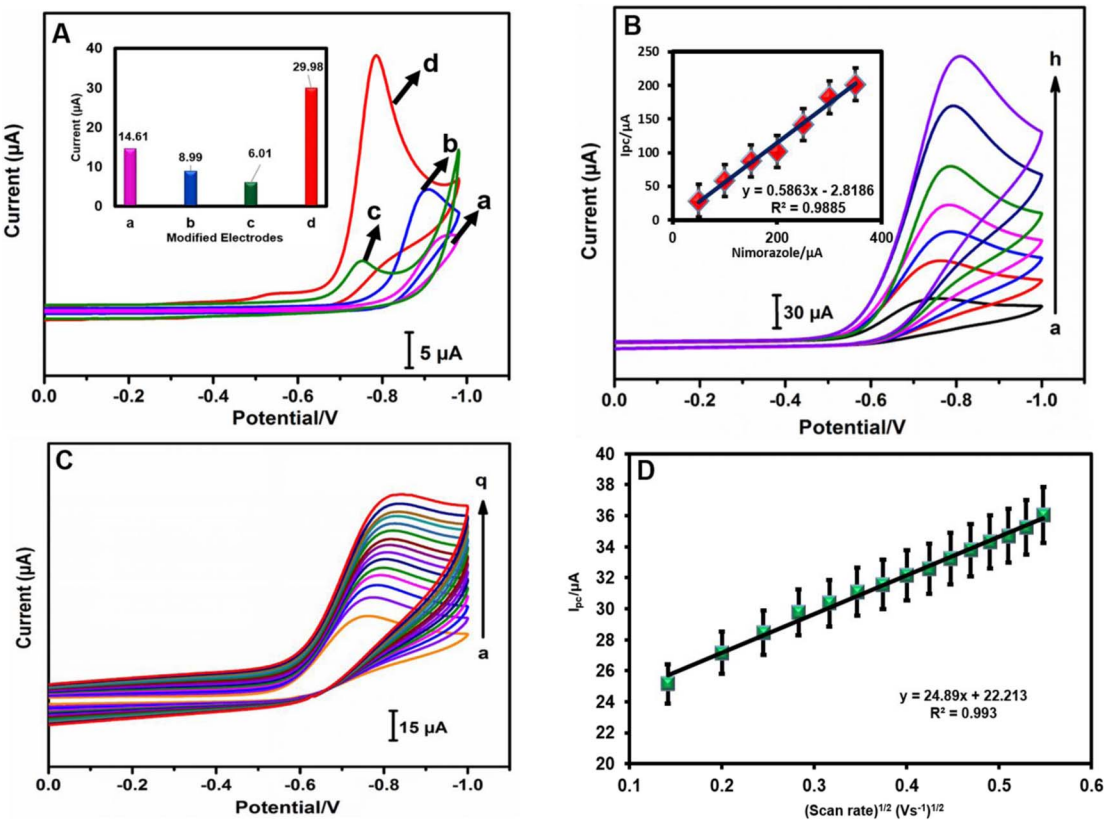

Figure 4. (A) CVs obtained at unmodified Bare SPCE (a), GO/SPCE (b), PB MCs/SPCE (c) and rGO/PB MCs/SPCE (d). (B) CVs acquired at rGO/PB MCs/SPCE in 0.1 M PB (pH 5) containing DMZ (a to h; 50 to 500 μM). Inset [DMZ]/μM vs. current/μA. (C) (scan rate)$^{1/2}$ (V.s–1)$^{1/2}$ vs. peak currents (μA) and (d) CVs obtained at rGO/PB MCs/SPCE in 0.1 M buffer (pH 5) containing 50μM of DMZ at different scan rates (a to q; 20 to 300 mVs-1).

The rGO/PB MCs/SPCE displayed greater electrocatalytic capability and electron transmissions as revealed by the improved cathodic peak currents at diminished over potential. The peak current acquired at rGO/PB MCs/SPCE was 3.5, 6.2, fold higher than those achieved at bare SPCE and GO/SPCE, respectively. (Figure 4B) Presents the CVs obtained at rGO/PB MCs/SPCE in Phosphate buffer (pH 5.0) headed for altered DMZ concentrations. The concentration of DMZ increases linearly as the increase in cathodic peak current (inset to Figure 4B). The reduction peak current is periodically improved as the increase in scan rate, which unveiled the signifying electrocatalytic property of the diffusion-controlled electrocatalytic process (Figure 4C). The good linearity verified the diffusion-controlled electrocatalytic process in the plot between reduction peak current and the square root of the scan rate displayed in (Figure 4D).

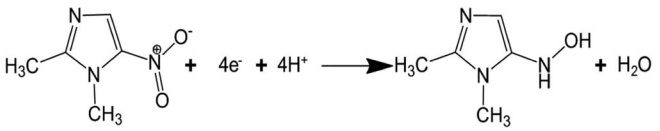

[1]

Interaction between DMZ and rGO/PB MCs.—The abundant PB cubes are formed and are closely held together. Due to this, massive amount of binding sites are buried and may also leads to decrease the DMZ adsorption amount in aqueous media. The water-compatible reduced graphene oxide acts as a key element of the sensor, which is wrapped all over the cubes to possess higher binding capacity, faster mass transfer and binding kinetics. Moreover, some functional groups positioned at the boundaries of rGO can deliver additional active sites for DMZ adsorption. Interaction between the DMZ and rGO/PB MCs is through the co-ordination bonding. Because, there is no obvious current signal when the CVs are obtained without DMZ. But, on addition of DMZ, the reduction peak current is attributed to the four-electron reduction of nitro group of aromatic and heteroaromatic nitro compounds to the corresponding hydroxylamine (Equation 1).

The influence of pH.—The pH influence on the electrocatalytic response of 50 μM DMZ at the rGO/PB MCs/SPCE is inspected by CV with phosphate buffer (0.1 M) within the pH range of 1.0–9.0. As can be seen in Figure 5, the *I*p increases with an increase of pH value from 3.0 to 5.0, then decreases with increasing pH value from 5.0 to 9.0. The maximum peak current is spotted at pH 5.0. Thus, the optimum pH of phosphate buffer is set at 5.0. The relationship between the reduction peak potential (*E*p) and pH is shown in Figure 5C. A linear shift of *E*p toward negative potential upon the increase of pH from 1.0 to 9.0 indicates that protons are directly involved in the reduction of DMZ and it obeys the following equation: *E*p = – 0.2450 – 0.0598 pH (R = 0.9971). The slope of –0.0598 V pH^{-1} is nearer to the theoretical value of – 0.0591 V pH^{-1} according to the Nernst equation, which proposes the contribution of equal numbers of electrons and protons in the electro-reduction of DMZ as specified in Equation 1.

Amperometric determination of DMZ.—(Figure 6A) showed the *i-t* curve acquired for rGO/PB MCs adapted electrode upon subsequent additions of 0.2, 5, 10, and 50 μM of DMZ into pH 5 at periodical intermissions of 50 sec (E_{app} = – 0.73 V, vs. Ag/AgCl). Steady and stable results are witnessed on each addition (Figure 6B), and the resulting current improved linearly as the DMZ concentrations increased. Therefore, the linear range is 0.02 μM to 1360.1μM. The limit of detection is 3.2 nM, and the sensitivity reached 2.2935 μAμM^{-1}cm^{-2}.

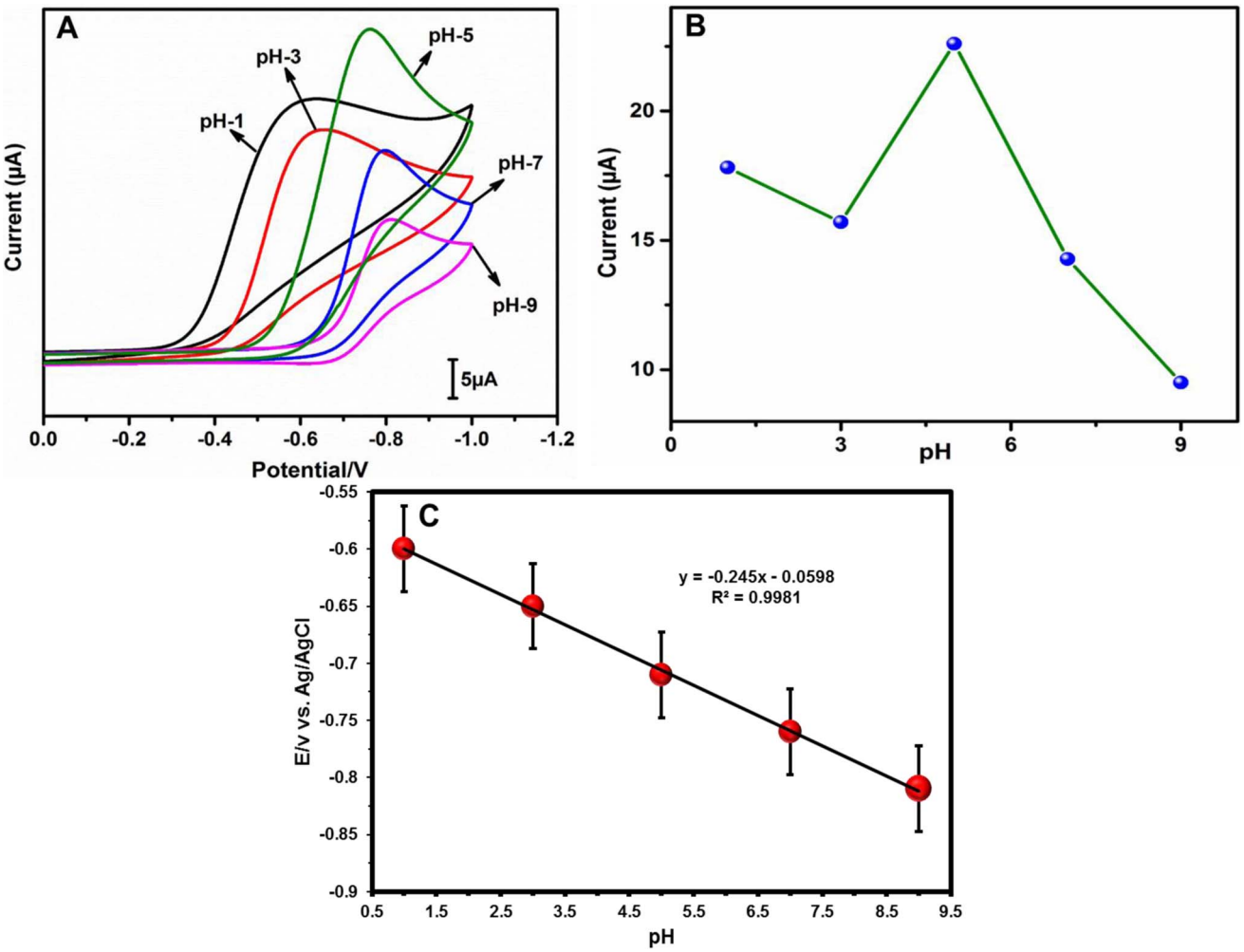

Figure 5. (A) CVs obtained for different pH solutions containing 50 μM DMZ at a scan rate of 0.50 V s^{-1}, (B) Plot of peak current (μA) vs. pH, and (C) Plot between peak potential (V) vs. pH For pH studies, the cyclic voltammograms are carried out in supporting electrolyte of different pH containing 50 μM DMZ at a scan rate of 0.50 V s^{-1}.

Selectivity towards DMZ.—The selectivity toward DMZ is considered by carrying out a study in the presence of co-existing interfering components. But, (Figure 6C) showed the choosy amperometric responses of rGO/PB MCs modified electrode to 0.005 mM of DMZ (a), 50 μM of Ronidazole (b), Amprolium (c), Tinidazole (d), Sulfacetamide (e), Sulfaguanidine (f), D-penicillamine (g), Doxycycline (h), and Clazuril (i). As a final point, the system selectively responded toward DMZ in the buffer, which is influenced by the mixture of interfering chemicals.

Reproducibility and durability.—The prepared electrode's responses were examined on a daily basis to observe the wearing ability (Figure 6D). The sensor maintained 98.2% of its first response even after a month, which authenticated the moral wearing consistency of the proposed electrode. On examining the reproducibility, CVs are obtained from 5 separate rGO/PB MCs modified electrodes in the buffer holding 0.01 mM of DMZ; the obtained relative standard deviation was 2.82%.

Real sample analysis (milk and egg samples).—The applied practicality of the system is verified in the samples of milk and egg. With the intention of analyzing milk samples, fresh milk (without DMZ) was added to phosphate buffer and stirred for 30 min. Then, the solution is spiked with identified quantities of DMZ, and the amperometric method was keep on executed (Figure 7C). The electrode distributed fast signals as laboratory samples. Finally, it owned the more extensive linear range for the milk sample between 0.031 and 1058.7 μM, and it acquired the LOD of 14.1 nM with the sensitivity of 2.499 $\mu A \mu M^{-1} cm^{-2}$ (Figure 7D). Food industrialists want indicative devices to confirm and quantifies the existence of DMZ, added for prophylaxis. Likewise, this method disclosed the practical applicability in DMZ spiked egg samples. As a final point, it possessed the wide-ranging linearity for the egg sample between 0.035 μM to 1069 μM and the attained LOD was 16.95 nM with the satisfactory sensitivity of 2.4235 $\mu A \mu M^{-1} cm^{-2}$ (Figures 7A, 7B). Satisfying the requirements for the cheap and responsive electrochemical device, here an advantage, as well as an instantaneous analytical device for the detection of DMZ in milk and egg samples, is developed.

Conclusions

An incredibly responsive, reproducible and hard-wearing DMZ detector is validated by the material, rGO/PB MCs. The composite is synthesized via the hydrothermal technique, and its efficient materialization is publicized by FE-SEM, XRD, EDX, EIS and electrochemical methods. The rGO/PB MCs/SPCE exhibited excellent electrocatalytic property toward DMZ reduction, and the sensor enactment was moreover better or equivalent to the literature.[6,20,22,24–28] The assay procedure was simple, reckless, and reproducible. This technique tends to be useful in the detection of DMZ contained in the

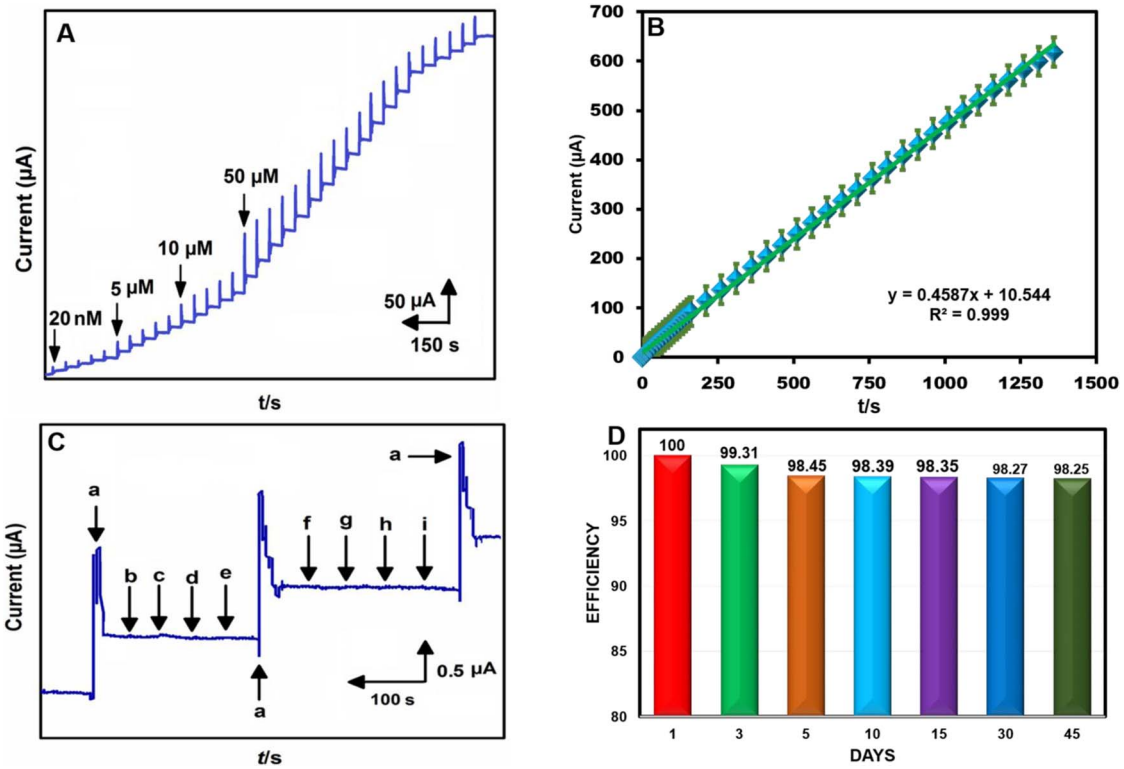

Figure 6. (A) Amperometric response of rGO/PB MCs film modified electrode for each sequential additions of DMZ into 0.1 M PB (pH 5). The rotation speed = 1200 RPM. (B) Plot of [DMZ]/μM vs. current (μA). *E*app = − 0.73 V (vs. Ag/AgCl). (C) Amperometric selective responses of rGO/PB MCs/SPCE toward 5 μM of DMZ (a) and 0.5 mM of Ronidazole (b), Amprolium (c), Tinidazole (d), Sulfacetamide (e), Sulfaguanidine (f), D-penicillamine (g), Doxycycline (h), and Clazuril (i).(D) Stability of rGO/PB MCs/SPCE as its continuous usage. The CV responses of rGO/PB MCs/SPCE toward 10 μM DMZ in 0.1 M PB (pH 5), monitored for the given number of days.

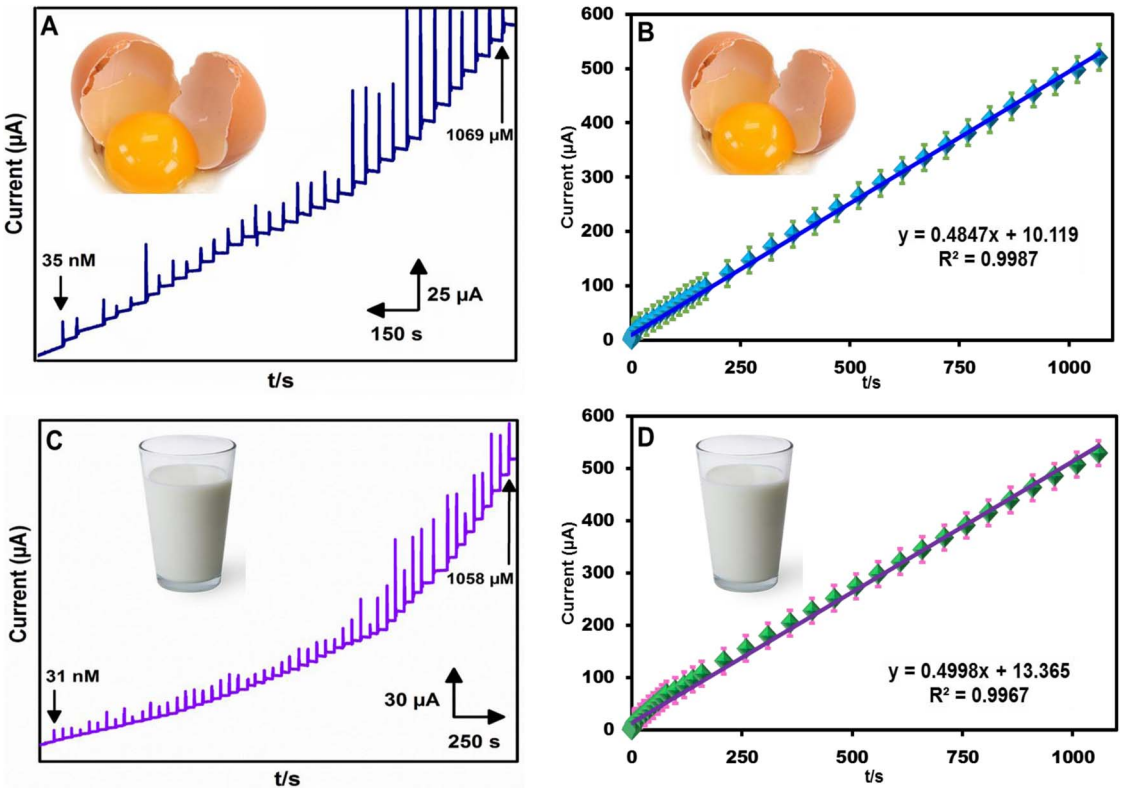

Figure 7. Amperometric response of rGO/PB MCs/SPCE for each sequential addition of real samples containing spiked DMZ into 0.1 M PB (pH 5.0). (A) Egg sample and, (C) Milk sample. Calibration plots for Egg (B) and Milk (D), $E_{app} = -0.73$ V (vs. Ag/AgCl).

Table I. Comparison of electroanalytical parameters obtained at rGO/PB MCs film modified electrode towards DMZ with previous reports.

Methods	Linear range	LOD	Ref.
HPLC-UV Detection	0–100 μM	0.5 μM	20
Gas chromatography-electron capture negative ionization mass spectrometry	-	0.1–0.6 μM	6
Liquid chromatography-Tandem mass spectrometry	0–10 μM	0.5 μM	21
Different pulse voltammetry	0.01 μM–1 μM	0.0036 μM	22
Different pulse voltammetry	0.5 μM–1000 μM	0.12 μM	23
Amperometric *-it*	**0.02 μM–1360.1 μM**	**0.0032 μM**	**This work**

samples of milk and egg. Moreover, it holds superior perspective in food preservative[29] and poultry farming welfares.

Acknowledgment

The authors appreciate the Deanship of Scientific Research at King Saud University for funding this work through research group no (RG-195). The authors extend their appreciations to the Ministry of Science and Technology and the Ministry of Education of Taiwan (Republic of China) and National Taipei University of Technology, Taipei, Taiwan supported this work.

References

1. T. L. Fodey, L. Connolly, S. R. Crooks, P. Delahaut, and C. T. Elliott, *Analytica chimica acta*, **483**, 193 (2003).
2. L. H. Stanker, C. McKeown, B. E. Watkins, M. Vanderlaan, R. Ellis, and J. Rajan, *Journal of agricultural and food chemistry*, **41**, 1332 (1993).
3. S. Kogularasu, M. Govindasamy, S.-M. Chen, M. Akilarasan, and V. Mani, *Sensors and Actuators B: Chemical*, **253**, 773 (2017).
4. M. Akilarasan, M. Govindasamy, S.-M. Chen, S. Kogularasu, and V. Mani, *Microchimica Acta*, 1 (2017).
5. M. Govidasamy, S. Kogularasu, Shen-Ming Chen, Yi-Hui Cheng, M. Akilarasan, and Mani Veerappan, *Journal of The Electrochemical Society*, **164**, B463 (2017).
6. C. Ho, D. W. Sin, K. Wong, and H. P. Tang, *Analytica chimica acta*, **530**, 23 (2005).
7. X. Huang, J. Lin, and D. Yuan, *Journal of separation science*, **34**, 2138 (2011).
8. A. K. Geim and K. S. Novoselov, *Nature materials*, **6**, 183 (2007).
9. D. A. Brownson, D. K. Kampouris, and C. E. Banks, *Journal of Power Sources*, **196**, 4873 (2011).
10. A. Kretinin, Y. Cao, J. Tu, G. Yu, R. Jalil, K. Novoselov, S. Haigh, A. Gholinia, A. Mishchenko, and M. Lozada, *Nano letters*, **14**, 3270 (2014).
11. D. Chen, H. Feng, and J. Li, *Chemical reviews*, **112**, 6027 (2012).
12. R. Kou, Y. Shao, D. Mei, Z. Nie, D. Wang, C. Wang, V. V. Viswanathan, S. Park, I. A. Aksay, and Y. Lin, *Journal of the American Chemical Society*, **133**, 2541 (2011).
13. Z.-S. Wu, S. Yang, Y. Sun, K. Parvez, X. Feng, and K. Müllen, *Journal of the American Chemical Society*, **134**, 9082 (2012).
14. B. Yuan, C. Xu, D. Deng, Y. Xing, L. Liu, H. Pang, and D. Zhang, *Electrochimica acta*, **88**, 708 (2013).
15. X.-J. Wang, F. Krumeich, and R. Nesper, *Electrochemistry Communications*, **34**, 246 (2013).
16. M. Pumera, A. Ambrosi, A. Bonanni, E. L. K. Chng, and H. L. Poh, *TrAC Trends in Analytical Chemistry*, **29**, 954 (2010).
17. D. A. Brownson and C. E. Banks, *Physical Chemistry Chemical Physics*, **13**, 15825 (2011).
18. H. Ming, N. L. Torad, Y.-D. Chiang, K. C.-W. Wu, and Y. Yamauchi, *CrystEngComm*, **14**, 3387 (2012).
19. P. J. Kulesza, M. A. Malik, A. Denca, and J. Strojek, *Analytical chemistry*, **68**, 2442 (1996).
20. M. J. Sams, P. R. Strutt, K. A. Barnes, A. P. Damant, and M. D. Rose, *Analyst*, **123**, 2545 (1998).
21. E. Daeseleire, H. De Ruyck, and R. VanRenterghem, *Analyst*, **125**, 1533 (2000).
22. C. Hu, J. Deng, X. Xiao, X. Zhan, K. Huang, N. Xiao, and S. Ju, *Electrochimica Acta*, **158**, 298 (2015).
23. Y. Gu, X. Yan, C. Li, B. Zheng, Y. Li, W. Liu, Z. Zhang, and M. Yang, *Biosensors and Bioelectronics*, **77**, 393 (2016).
24. G. Yang and F. Zhao, *Sensors and Actuators B: Chemical*, **220**, 1017 (2015).
25. P. Cooper and R. Hoodless, *Analyst*, **92**, 520 (1967).
26. A. Hobson-Frohock and J. A. Reader, *Analyst*, **108**, 1091 (1983).
27. M. J. Parnell, *Pest Management Science*, **4**, 643 (1973).
28. D. Hughes, *Journal-Association of Official Analytical Chemists*, **71**, 474 (1987).
29. T. V. Duncan, *Journal of colloid and interface science*, **363**, 1 (2011).